

## ASSESSMENT OF THE CAPABILITY OF 3D STRATIFIED FLOW FINITE ELEMENT MODEL IN CHARACTERIZING MEANDER DYNAMICS

Dwinanti R. Marthanty<sup>1,2\*</sup>, Herr Soeryantono<sup>1</sup>, Erick Carlier<sup>2</sup> and Dwita Sutjiningsih<sup>1</sup>

<sup>1</sup>Department of Civil Engineering, University of Indonesia, Indonesia

<sup>2</sup>Ecole Polytech Lille, University Lille 1, France

Received 11 June 2014; received in revised form 11 December 2014; accepted 12 December 2014

### Abstract:

There have been attempts to simulate meander dynamics (Langbein & Leopold, 1966; Oodgard, 1989; Campoerale *et al.*, 2007; da Silva & El-Tahawy, 2008; Duan & Julien, 2010; Blanckaert & de Vriend, 2010; Esfahani & Keshavarzi, 2011). Meandering geometry is complex phenomena (Chanson, 2004; Wu, 2008), this would include the dynamics of flow properties and of morphology. Simulating meander flow dynamics is mostly popular using either Finite Element Method (FEM) or Finite Volume Method (FVM) where are based on Eulerian description, and based on stationer grid-based methods (Wormleaton & Ewunetu, 2006; Wu, 2008; Duan & Julien, 2010; Gomez-Gesteira *et al.*, 2010). As such this model is lack of capability in simulating the dynamics of meander morphology; much effort is put through to overcome this issue with such as Smoothed Particle Hydrodynamics (SPH), Boundary Element Methods, Arbitrary Lagrangian Eulerian, etc. This paper has two objectives; to identify meander flow characteristics and sediment transport distribution patterns, and to simulate meander flow characteristics and sediment transport distribution patterns using FEM. This study has identified that the key of dynamics of flow characteristics are helical flow and coherent structures, and the key of dynamics of transport characteristics are erosion-deposition zone patterns. The finite element model using in this study, RMA has shown its capability to simulate the meander key characteristics above, for small deflection angles (30°) location of maximum erosion-deposition zones near the crossover of the sinuosity, for intermediate deflection angles (70°) location of maximum erosion-deposition zones between the crossover and apex of the sinuosity, and for large deflection angles (110°) location of maximum erosion-deposition zones near the apex of the sinuosity, these are agreed with experiments of Odgaard (1989), da Silva (2006), da Silva *et al.* (2006) and Esfahani & Keshavarzi (2012). These results can be used as a reference to develop a method to model meander morpho-dynamics.

**Keywords:** meander dynamics; flow structures; helical flow; sediment transport; sedimentation; deposition; finite element methods; RMA-10; RMA-11;

© 2014 Journal of Urban and Environmental Engineering (JUEE). All rights reserved.

\* Correspondence to: Dwinanti Rika Marthanty, Tel.: +628567233297. E-mail: [dwinanti@eng.ui.ac.id](mailto:dwinanti@eng.ui.ac.id)

## INTRODUCTION

Meandering phenomena have been attracted many researches to simulate its dynamics (Langbein & Leopold, 1966; Oodgard, 1989; Campoerale *et al.*, 2007; da Silva & El-Tahawy, 2008; Duan & Julien, 2010; Blanckaert & de Vriend, 2010; Esfahani & Keshavarzi, 2011). Einstein started to explain the cause of formation of meanders in 1926. The circular movement still exists at cross-section of its course even without bends and sediment transport. It is caused by large-scale turbulence (Leopold & Wolman, 1957; da Silva, 2006; Vickers *et al.*, 2008; Riley and Rhoads, 2012).

Meandering dynamics deal with the study of river flow and sediment problems which are very complex phenomenon and large scale system, therefore finding analytical solutions is very difficult (Wu, 2008). According to Camporeal (2007), the fundamental elements of meandering are the curvature of the channel axis and the erodibility of the bed and banks. da Silva (2006) also mentions the pertinent aspects of the meander geometry based on artificial geometry of sine-generated curve. In nature, meandering geometry is more complicated.

Simulating meander flow dynamics is mostly popular using either Finite Element Method (FEM) or Finite Volume Method (FVM) where are based on Eulerian description, and based on stationer grid-based methods (Bates *et al.*, 2005, Wendt, 2009). As such this model is lack of capability in simulating the dynamics of meander morphology many effort is put through to overcome this issue with such as Smoothed Particle Hydrodynamics (SPH), Boundary Element Methods, Arbitrary Lagrangian Eulerian, etc. Recently SPH has been developed for free surface flow where this relatively new method has been chosen for its mesh-free domain (Shao & Gotoh, 2005; Aristodemo *et al.*, 2010). Particularly SPH is a robust and powerful method for describing deforming media in free surface flow (Gomez-Gesteira *et al.*, 2010).

Therefore in general, two approaches are used in morpho-dynamics simulation; stationer geometry (grid-based methods) and dynamic geometry (mesh-free methods).

FEM is one of classical numerical methods where it is bound to rigid domain model. King (2012, 2013) developed a finite element model for three-dimensional flow and is called Resource Modelling Associates (RMA), for density stratified flow (RMA-10) and for water quality in estuaries and streams (RMA-11). It is suited for computing the hydrodynamics of shallow water flow and limited to uniform sediment (Papanicolaou *et al.*, 2008).

The development of meander model has to have a capability to simulate meander flow characteristic and sediment transport distribution pattern, at least having the same capability as the finite element method (Wu,

2008; da Silva, 2006). Here, the meander flow is characterized by having helical flow and coherent structures (bursts and sweeps), higher flow velocity at the outer banks and lower in the inner banks, sediment erosion at the outer banks and deposition in the inner banks, higher sediment concentration at the outer banks and lower in the inner banks.

This paper has two objectives; to identify meander flow characteristics and sediment transport distribution patterns, and to simulate meander flow characteristics and sediment transport distribution patterns using FEM with RMA. These results can be used as a reference to develop a method to model meander morpho-dynamics.

## IDENTIFICATION OF FLOW MEANDER CHARACTERISTICS AND SEDIMENT TRANSPORT DISTRIBUTION PATTERNS

Flow in meanders is classified as three-dimensional, incompressible, having free surface and movable bed and banks, turbulent, and the presents of helical flows. In meanders, the flow velocity is decreasing at the bends and sidewalls by the occurrence of secondary currents, which diverse the velocity distribution. Secondary currents are perpendicular to the main current and they are caused by Reynolds stresses in any noncircular conduits (Chanson, 2004). The major secondary current observed in the cross-section of a channel bend is the helical flow, which exists due to the difference between the centrifugal forces in the upper and lower flow layers, and points to the outer bank in the upper layer and to the inner bank in the lower layer. Other secondary flow cells exist as eddies and appear in coherent structures due to anisotropic turbulence (Wu, 2008). Coherent turbulence structures in meanders, called bursts and sweeps, are responsible for transferring fluid momentum across local velocity gradients (Gunalp *et al.*, 2012; da Silva and Ahmari, 2009). Gunalp *et al.* (2012) found that bursts are oriented towards inner-bank and sweeps are oriented towards outer-bank of the channel bend.

da Silva & Ahmari (2009) found that the formation of large-scale river forms is directly related to the large-scale turbulence, particularly the formation of alternate bars and meanders through the actions of horizontal coherent structures on the mean flow and the mobile bed and banks. This is agreed with Mao (2003) experiments that at high roughness Reynolds number the bursts and sweeps phenomena can send sediment particles into suspension where bed forms and bed roughness interact with the coherent turbulent structures and resulted in flow and sand movement in alluvial rivers. The most recent result comes from Esfahani & Keshavarzi (2012), they detected the importance of sweeps and bursts on sediment deposition, and stated the occurrence of fluctuating velocities in three-dimensions inside meanders is responsible for sediment transport. Based on da Silva (2006) experiments, it is

found that the stronger the intensity of convergence-divergence of flow, the deeper will be the erosions at the bed and the stronger the direct action of flow on the banks – and, consequently, the larger the lateral expansion velocity. The location of erosion-deposition zones is to vary with deflection angles (Esfahani & Keshavarzi, 2012). From that perspective, we can expect that the zones of erosions and depositions coincide with the zones of convective acceleration and deceleration of flow respectively.

**NUMERICAL EXPERIMENT WITH RMA**

The governing equations of RMA-10 is based on the combination of the Reynolds form of the Navier-Stokes equations, the volume continuity equation, the advection diffusion equation, and an equation of state relating water density to salinity or temperature. For fully three-dimensional model, the required boundary conditions that must be defined here are water surface elevation, sediment concentration, sediment flux, and specified velocity at land and water boundaries. Practically it can be divided into three categories which are the free surface, the bed, and the side boundaries. RMA-10 is using isoparametric approximations to define elements, Galerkin Method of Weighted Residuals for the finite element derivation, Newton-Rhapson method to structure and iterate for the nonlinearity, modified Crank-Nicolson time stepping scheme for unsteady flow, and Gaussian quadrature to integrate the finite element integrals. Hydrostatic pressure assumption is considered since vertical momentum effects may be neglected and the vertical velocities are sufficiently small (King, 1993; 2012). RMA-11 is a finite element water quality model to simulate three-dimensional estuaries, bays, lakes and rivers as separate system or combined form. It employs the input of velocities and depths from RMA-10 for the computation of advection diffusion constituent transport equations with additional terms for each source/sink and growth/decay.

**Governing Equations for three-dimensional stratified flow**

RMA-10 uses three-dimensional stratified flow equations describing velocity in all three Cartesian directions, water pressure and the distribution of constituent concentration of sediment throughout the system. The sediment is treated as the dependent variable.

$$\text{Volume Continuity: } \frac{\partial u_j}{\partial x_j} = 0 \tag{1}$$

$$\text{Momentum equation: } \rho \left( \frac{\partial u_i}{\partial t} + u_j \frac{\partial u_i}{\partial x_j} \right) - \frac{\partial}{\partial x_j} \left( \epsilon_{x_j x_j} \frac{\partial u_i}{\partial x_j} \right) + \frac{\partial p}{\partial x_i} - \Gamma_{x_i} = 0 \tag{2}$$

Advection Diffusion: (3)

$$\frac{\partial c}{\partial t} + u_j \frac{\partial c}{\partial x_j} - \frac{\partial}{\partial x_j} \left( D_{x_j} \frac{\partial c}{\partial x_j} \right) - \theta_s = 0$$

$$\text{Hydrostatic Approximation: } \frac{\partial p}{\partial z} + \rho g = 0 \tag{4}$$

where *i, j* are general coordinate directions as subscripts, *u<sub>j</sub>* is the component vector velocity in *j*-direction, *x<sub>j</sub>* is coordinate system in *j*-directions, *ρ* is density, *ε<sub>*x<sub>j</sub>x<sub>j</sub>*</sub>* is the turbulent eddy coefficients, *u<sub>i</sub>* is the vector velocity in *i*-direction, *t* is for time, *p* is for pressure, *Γ<sub>*x*</sub>* is external forces, *c* is constituent concentration, *D<sub>*x*</sub>* is the eddy diffusion coefficients, and *θ<sub>*s*</sub>* is the source/sink for the constituent. In the RMA-10 formulation of the vertical velocity *w* is used only in the two momentum equations and the advection diffusion equation. For the simulation model, the main dependent variables are thus the horizontal velocity components *u* and *v*, the water depth *h* and the constituent concentration *c*.

For **Eqs (1) through (4)**, the geometric system varies with time where the water depth *h* varies during the simulation. In modifying the geometry the transformation is defined by *a* as the elevation of the bottom relative to the same vertical datum and *b* as the fixed vertical location to which the water surface will be transformed. To add in the impact of the transformation, the horizontal eddy coefficients have been modified but neglected the influence of slightly non horizontal diffusion induced by the transformation.

The final form for three-dimensional stratified flow that is used in RMA-10 and developed by King (1993) are momentum **Eqs (5) and (6)**, volume continuity **Eq. (7)**, advection diffusion **Eq. (8)**, and equation of state **(9)**:

$$\rho \left\{ \begin{aligned} &h \frac{\partial u}{\partial t} + hu \frac{\partial u}{\partial x} + hv \frac{\partial u}{\partial y} + \\ &\frac{\partial u}{\partial z} \left[ (b-a)(w - uT_x - vT_y) - (z-a) \frac{\partial h}{\partial t} \right] \end{aligned} \right\} - \tag{5}$$

$$(b-a) \frac{\partial}{\partial x} \left[ \epsilon_{xx} \frac{h}{(b-a)} \frac{\partial u}{\partial x} \right] -$$

$$(b-a) \frac{\partial}{\partial y} \left[ \epsilon_{xy} \frac{h}{(b-a)} \frac{\partial u}{\partial y} \right] - (b-a) \frac{\partial}{\partial z} \left[ \epsilon_{xz} \frac{\partial u}{\partial z} \right] +$$

$$\rho_s gh \frac{\partial a}{\partial x} + \rho_s gh \frac{\partial h}{\partial x} + g_x h - h\Gamma_x = 0$$

$$\rho_s \left\{ h \frac{\partial v}{\partial t} + hu \frac{\partial v}{\partial x} + hv \frac{\partial v}{\partial y} + \frac{\partial v}{\partial z} \left[ (b-a)(w - uT_x - vT_y) - (z-a) \frac{\partial h}{\partial t} \right] \right\} \quad (6)$$

$$(b-a) \frac{\partial}{\partial x} \left[ \epsilon_{yx} \frac{h}{(b-a)} \frac{\partial v}{\partial x} \right] - (b-a) \frac{\partial}{\partial y} \left[ \epsilon_{yy} \frac{h}{(b-a)} \frac{\partial v}{\partial y} \right] - (b-a) \frac{\partial}{\partial z} \left[ \epsilon_{yz} \frac{\partial u}{\partial z} \right] + \rho_s gh \frac{\partial a}{\partial y} + \rho_s gh \frac{\partial h}{\partial y} + g_y h - h\Gamma_y = 0$$

$$\left[ \frac{\partial u}{\partial x} - \frac{(b-a)}{h} \frac{\partial u}{\partial z} T_x + \frac{\partial u}{\partial y} - \frac{(b-a)}{h} \frac{\partial v}{\partial z} T_y \right] dz + \int_a^b u_s \frac{\partial(a+h)}{\partial x} - u_b \frac{\partial(a)}{\partial x} + v_s \frac{\partial(a+h)}{\partial y} - v_b \frac{\partial(a)}{\partial y} + \frac{\partial h}{\partial t} = 0 \quad (7)$$

$$h \frac{\partial c}{\partial t} + hu \frac{\partial c}{\partial x} + hv \frac{\partial c}{\partial y} + \frac{\partial c}{\partial z} \left[ (b-a)(w - uT_x - vT_y) - (z-a) \frac{\partial h}{\partial t} \right] - (b-a) \frac{\partial}{\partial x} \left( D_x \frac{h}{(b-a)} \frac{\partial c}{\partial x} \right) - (b-a) \frac{\partial}{\partial y} \left( D_y \frac{h}{(b-a)} \frac{\partial c}{\partial y} \right) - (b-a) \frac{\partial}{\partial z} \left( D_z \frac{\partial c}{\partial z} \right) - h\theta_s = 0$$

$$\rho - F(c) = 0 \quad (9)$$

where  $\rho_s$  is the density at the surface;  $\rho_z$  is the density at the elevation  $z$ ;  $u_s$  and  $v_s$  are horizontal Cartesian velocity components at the water surface; and  $u_b$  and  $v_b$  are horizontal Cartesian velocity components at the bed. It is noted that the momentum and advection diffusion equations have been multiplied by  $h$ .  $D_x$ ,  $D_y$ , and  $D_z$  represent similar approximations for the diffusion coefficients to those were made for the eddy coefficients.  $T_x$ ,  $T_y$ ,  $g_x$ , and  $g_y$  are defined by:

$$T_x = \frac{\partial a}{\partial x} + \frac{(z-a)\partial h}{(b-a)\partial x} - \frac{h}{(b-a)} \frac{\partial a}{\partial x} + \frac{(z-a)}{(b-a)^2} h \frac{\partial a}{\partial x} \quad (10)$$

$$T_y = \frac{\partial a}{\partial y} + \frac{(z-a)\partial h}{(b-a)\partial y} - \frac{h}{(b-a)} \frac{\partial a}{\partial y} + \frac{(z-a)}{(b-a)^2} h \frac{\partial a}{\partial y} \quad (11)$$

$$g_x = \int_z^{a+h} \frac{\partial}{\partial x} (\rho g) dz \quad (12)$$

$$g_y = \int_z^{a+h} \frac{\partial}{\partial y} (\rho g) dz \quad (13)$$

### Boundary and Initial Conditions

The free water surface is no leakage boundary conditions across the surface and zero pressure where the water depth is  $h$ .

$$w_s = \frac{dh}{dt} \quad (14)$$

The bottom is no leakage condition with drag from the bed for velocities:

$$u_b \frac{\partial a}{\partial x} + v_b \frac{\partial a}{\partial y} - w_b = 0 \quad (15)$$

where  $u_b$ ,  $v_b$ , and  $w_b$  are represent Cartesian velocity components at the bottom, and  $a$  is the elevation of the bottom relative to the same vertical datum. The side boundaries occur at system cuts where the boundary conditions specify water surface elevations for each  $(x,y)$  location, velocities at the  $(x,y,z)$  location, or flows at the cuts ( $u_h$  and or  $v_h$ ). The boundary is considered as being at a fixed location, thus it will require special numerical and analytical techniques for moving boundary systems.

Surface tractions for bed friction are using Chezy friction equation:

$$\Gamma_x = -\frac{\rho g u_b V}{c^2}, \quad \Gamma_y = -\frac{\rho g V_b V}{c^2} \quad (16)$$

RMA-10 formulation for vertical eddy viscosity and diffusivity is based on diffusivity distributions developed for stratified reservoirs application.

### MODEL SET-UP

The value of parameter in model set up can be selected from a feasible range, evaluated in the model, adjusted to the model results based on literature review and/or pervious modeling studies and experimental data (Ji, 2008).

RMA model consists of simulation sequence and graphic modules. The pre-processor is RMAGEN which is a graphic module to generate mesh of finite element networks. The processor for three-dimensional finite element model for stratified hydrodynamic simulation is RMA-10, and for three-dimensional water quality model including sediment transport is RMA-11. The post-processor is RMAPLT for displaying results as current vectors, contour plots, time histories or section plots.

The processor modules of RMA-10 and RMA-11 are based on the finite element method and geometrically designed to execute input setting from two-dimensional

horizontal network and data describing the number of elements vertically from all corner nodes.

The processor file structures can be seen as series of blocks as seen in Fig. 5. The input files of RMA-10 and RMA-11 are similar. There is only one addition R4Q file need to describe the water quality parameters containing their relationships and kinetics.

**Meander Geometry**

For plan shape of a meandering river, we used sine-generated curve (Leopold & Langbein, 1966) as depicted by the following equation where  $l_c$  is longitudinal coordinate along the meandering flow centerline  $L$ :

$$\theta = \theta_0 \cos\left(2\pi \frac{l_c}{L}\right) \quad (17)$$

The best given proportionality of meander wavelength  $\Lambda_M$  and channel width  $B$  is around 6. The plan shapes of sine-generated curve are differed by values of the deflection angle  $\theta_0$ . The deepest erosions and highest depositions must be expected to occur around the crossovers  $O_i$  if  $\theta_0$  is “small”, and around the apex-sections  $a_i$  if  $\theta_0$  is “large”. Small angle is  $30^\circ$ , large angle is  $110^\circ$ , and medium angle is  $70^\circ$  (da Silva, 2006). Factors that affect the development of helical flow in this model are geometry characteristics and turbulence flow properties. The idea is to make the flow high turbulent in order to evoke helical flow. Therefore we set up high value of Smagorinsky closure for the flow and high Chezy friction number for the bed and wall.

**Mesh Generating and Bed Deformation**

Mesh is generated by a pre-processor module RMAGEN. Basically each element is a quadrilateral element with 8 nodes which are consisted of 4 corner nodes at the vertices of the element and 4 mid-side nodes in the middle of the element. Each cross-section channel is divided into 8 elements by width. For flat bed, it used bed depth 5.5 m or bed at elevation -5.5 m.

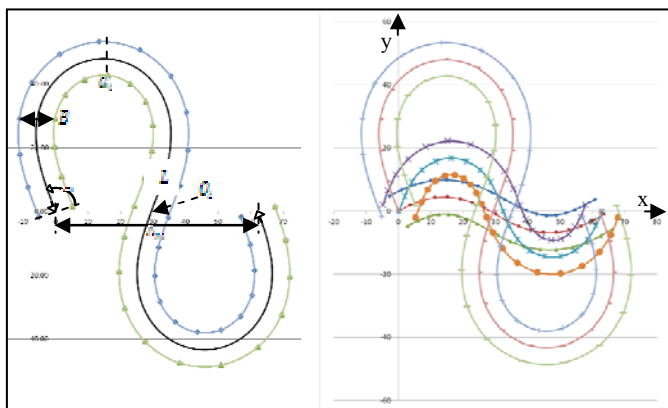


Fig. 1 Definition sketch of a meander geometry and bed depth contour. Unit in x and y directions are in meters.

Table 1. Variables of meander geometry.

Deflection angle of a meander-ing flow	$\theta_0$	$L$ [m]	$\Lambda_M$ [m]	$B$ [m]	Node Numbers	Element Numbers	Layer Numbers
Small	$30^\circ$	68	66	11	6185	2208	4
Medium	$70^\circ$	95	66	11	6905	2464	4
Large	$110^\circ$	232	66	11	8345	2976	4

In meander river, the bed is deformed at the bend where the inner bend has a higher level than the outer. The bed deformation gives significant effect in the development of helical flow since it governs the interaction between the turbulent flow motion and the suspended sediment constituting the river bed (Struiksma *et al.*, 1985).

**Simulation three-dimensional flow**

For the truly three-dimensional computation, RMA-10 uses the solid elements for the volume integrals and the surface elements for the boundary integrals. Types of surface elements used here are: (1) water surface elements for evaluation of surface velocity terms in the continuity equation; (2) bed elements for evaluation of bed friction and pressure terms in the momentum equations and bed velocity terms in the continuity equation; (3) side elements for external sides of system and applying pressure or water depth and or slip boundary conditions in the momentum equations.

The main inputs in RMA-10 are meander geometry, running control, system properties, initial condition, and transient step data. The meander geometries comprise flat and deformed beds for each deviation angle small, medium and large.

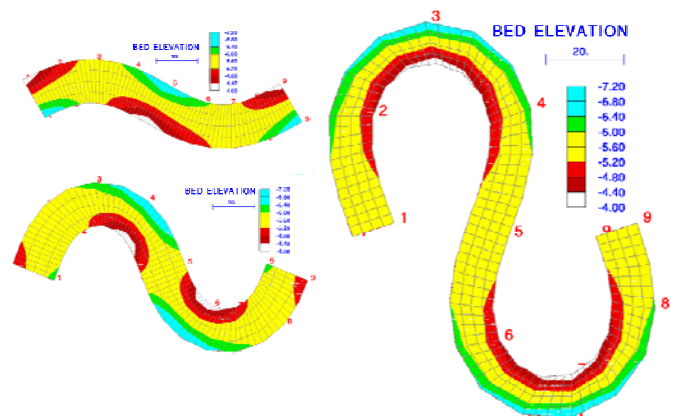


Fig. 2 Meshing elements, bed depth contours and continuity lines for deviation angles: (a)  $30^\circ$ , (b)  $70^\circ$ , and (c)  $110^\circ$ .

In control data block we set up turbulence closure method using original Smagorinsky to control horizontal eddy with alfa factor 0.5 and minimum kinematic eddy viscosity  $1.0 \text{ m}^2/\text{s}$ , using bottom friction Manning resistance to control bottom velocities, treating concentration variable as passive conservative constituent, local attitude average is 0.00 to set equator location, initial value for temperature is  $20^\circ\text{C}$  and for suspended sediment concentration is  $10.0 \text{ mg/l}$ , initial iteration value for  $u$  and  $v$  bed velocity is  $0.1 \text{ m/s}$ , initial water surface elevation is  $-2.0 \text{ m}$ , and suspended sediment settling rate is  $0.01 \text{ m/s}$ .

During convergence test, the maximum allowable change in  $x$ -velocity and  $y$ -velocity is  $0.02 \text{ m/s}$ , in temperature is  $0.010^\circ\text{C}$ , and in sediment is  $0.010 \text{ mg/l}$ .

As for element properties data, turbulent exchange coefficients associated with  $x$ -direction shear of  $x$ -direction flow, with  $y$ -direction shear of  $x$ -direction flow, and with  $x$ -direction shear of  $y$ -direction flow is all  $0.1 \text{ pascal-sec}$ , whether with  $y$ -direction shear of  $y$ -direction flow is  $1 \text{ pascal-sec}$ . Manning coefficient for all element is  $0.040$ , and turbulent exchange coefficients associated with  $z$ -direction shear of  $x$ -direction flow and with  $z$ -direction shear of  $y$ -direction flow is all  $0.1 \text{ pascal-sec}$ . Turbulent diffusion coefficient associated with the  $x$ -direction is  $0.05 \text{ m}^2/\text{s}$ , and Turbulent diffusion coefficient associated with the  $y$ -direction and with the  $z$ -direction is all  $0.1 \text{ m}^2/\text{s}$ . Manning coefficient for shoreline is  $0.020$ , and for water surface is  $0.015$ .

Vertical distribution coefficient at externally specified flow boundaries is  $0.4$ , and at interface between two- and three-dimensions is  $0.4$ . Here, we used 4 layers data at elevation  $-2.5 \text{ m}$ ,  $-3.0 \text{ m}$ ,  $-3.5 \text{ m}$ , and  $-5.0 \text{ m}$ .

For time variable simulation, firstly we simulated for steady state where time step is  $0$ . For transient state, time step is different for each geometry. The smaller the deviation angle is the smaller the time step. As for small deviation angle  $30^\circ$  is  $0.001 \text{ s}$ , for  $70^\circ$  is  $0.01 \text{ s}$ , and for  $110^\circ$  is  $0.05 \text{ s}$ .

In each geometry, it has 9 continuity lines where we set it up as boundary condition to determine the total flow and constituent inflow crossing the line. Otherwise, we used hydrograph inflow as dynamic simulation.

RMA-10 in fact can simulate a suspended sediment simulation along with the three-dimensional flow computation by using BQD option. However, after several running test, the results are not satisfied then we focus on RMA-11 simulation.

During the dynamic simulation, we used hydrograph values for the inflow with HYD file which is activated by LABL option with 1. The crucial parameters that has to be carefully input are TBFACT or alfa factor applied in Smagorinsky closure, TBMIN or minimum kinematic eddy viscosity using the Smagorinsky closure in  $\text{m}^2/\text{s}$ ,

INIT ELEV or initial water surface elevation, LD3 or layer data for specified elevations, and DT or time step control.

Smagorinsky model is chosen because it facilitates possible large-scale turbulence anisotropy (van Balen *et al.*, 2010). Initial water surface elevation is maintained to be valid for shallow water approximation when ratio of depth ( $h$ ) to channel length ( $L$ ) is less or equal to  $0.05$  (Ji, 2008). Time step control is kept below the flood wave travel time in order to stabilize the numerical calculation (Bates *et al.*, 2005; King, 2012).

$$\text{Shallow water approximation: } \frac{h}{L} \leq 0.05 \quad (18)$$

$$\text{Wave travel time: } \frac{L}{\sqrt{g * h}} \quad (19)$$

As stated by Ji (2008), based on sensitivity tests with a six-layer model, three-layer model is actually adequate to represent the vertical structure of the object study of surface water in most of the time.

### Simulation three-dimensional sediment transport

RMA-11 is using input of velocities and depths from RMA-10 output. RMA-11 used R4Q file to define input sediment parameters. The crucial parameters that has to be carefully input are defining diffusion DF in the properties block, setting up boundary conditions BC at the upstream, applying element loading DL whether at this time it is only for an element for three-dimensional simulation, setting conservative constituent to avoid bumpy results with ICNSV is 1, managing time step control DT lower than the wave travel to evade from low flow case, and specifying sediment parameters in R4Q file.

The diffusion coefficient (diffusivity) is often assumed to proportional to the eddy viscosity of turbulent flow. The parameters used in the model are horizontal and vertical eddy diffusivity coefficients. The horizontal eddy viscosity affects velocity distribution and can be calculated using the Smagorinsky scheme. The vertical eddy viscosity treats vertical mixing in the model and is represented in the closure model (Wu, 2008).

The zone of influence of boundary conditions propagates through the domain at each time step, and carries information from the upstream boundary condition. This is important in advection-dispersion problems where conservation of mass is considered certain (Julien, 2002).

Sediment can be assumed as a conservative constituent that do not react under chemical and biological decay where the rate of reaction is very low. The vertical velocity for cohesive sediment can be related to sediment concentration other factor such as

flow shear. The settling velocity for non-cohesive sediment is a function of the grain size, density, and shape, and is not customarily associated with sediment concentration (Ji, 2008).

Sediment is moved as suspended load and/or bed load. Cohesive sediments are only transported as suspended sediment whereas non-cohesive sediments can be both. Suspended load is transported in suspension in the water column including sediment resuspended from the bed and the wash load brought from upstream. Bed load is moved on or near the bed saltation, rolling, or sliding in the bed layer and occurs periodically in a thin layer of several grain diameters in thickness (Ji, 2008). It depends on their particles sizes to move in as suspended load or bed load, but it is commonly assumed suspension as the main transport mode (Wu, 2008).

Non-cohesive sediments on average include gravel, sand, and some silt. There are three important properties of non-cohesive sediments consist of (1) particle size, (2) shape, and (3) specific gravity (Ji, 2008).

Parameters of non-cohesive sediment used here are in line SAND1 there are minimum grain size 0.1 mm, maximum grain size 1.0 mm, specific gravity of sediment 2.65, grain shape factor 0.7, characteristics length factor/time for deposition 1.00, characteristics length factor/time for deposition 10.0, fall velocity for sediment 0.05 m/s, and Manning coefficient used to calculate bed shear velocity for Ackers-White formulation 0.02.

In line SAND2 there are D35 grain size 0.15 mm, D50 grain size 0.30 mm, D90 grain size 0.90 mm, transport method option to use Ackers and White is 1, and treatment of characteristics length factor/time for erosion-deposition option to use standard STUDH method is 0.

## RESULTS AND DISCUSSION

Results of RMA-10 and RMA-11 are presented in ASCII output files, and read by post-processor of RMAGEN. The simulations run on flat and deformed bed, with high and low flow, and for non-cohesive (sand).

The discussion object is divided in to three parts; flow structures, bed depth profiles, and sediment distributions.

For the turbulence structures through planform geometry, the cross-circulation flow combined with longitudinal flow motion defines helical flow. The presence of helical flow as shown in **Table 2** diverts the distribution of fluid velocity, and transfers the high momentum fluid from the inner-side to the outer-side of the river bend to shift the core of maximum velocity towards the outer-bank and the flow is accelerated. Towards the inner-bank, the flow is decelerated.

In **Fig. 3**, from the velocity vector fields the velocity is decreasing at the bends and sidewalls. This is agreed

with da Silva (2006), Tilston *et al.*, (2009), Termini and Piraino (2010) that the cause of decreasing velocity is the occurrence of helical flows. We can see from **Fig. 3** that the flow velocity gained the highest value at the outer bend for each deflection angle. The fluid flows from left to right, from this perspective the outer-bank is at the upper side of the curved-channels.

The deflection angle of sine-generated curve where flow enters the bend alters the shifting of velocity zones. The bigger the deflection moves the location of maximum velocity more downward of stream flow this can be seen in **Fig. 3**. According to Julien (2003) where he mentioned that the strength of secondary circulation is affected by the flow deviation angle of the streamlines. The deflection angle defines the deviation angle, where at large deviation angle shifts the maximum velocity zones and determine the direction of channel migration. This is also agreed with Odgaard (1989).

Through the water column, the high momentum fluid transfers from the upper-part of the flow towards the lower-part and it is called sweep. The opposite occurs along the tailing half of the rotation eddy, and it is known as burst. Sweep is oriented towards the outer-bank at acceleration zones, and burst is oriented towards the inner-bank at deceleration zones. Shown in **Table 2** this is agreed with Wu (2008) and Termini & Piraino (2010) where the major secondary current observed in the cross-section of a channel bend is the helical flow, and points to the outer bank in the upper layer and to the inner bank in the lower layer. For small deflection angle, the helical flow is developed clearly in cross-section 3 and consistent to spin clockwise direction up to cross-section 7. For medium deflection angle, the helical flow spun clockwise direction is also developed clearly in cross-section 3, but getting weaker in cross-section 5, and then developed stronger up to cross-section 8. For large deflection angle, the helical flow

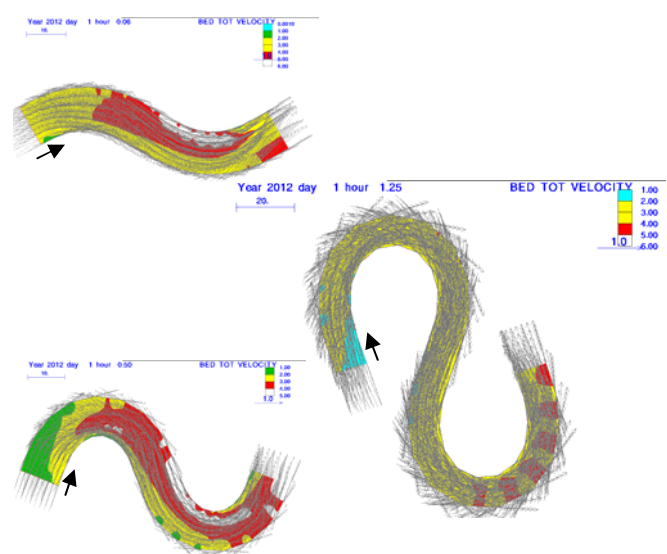
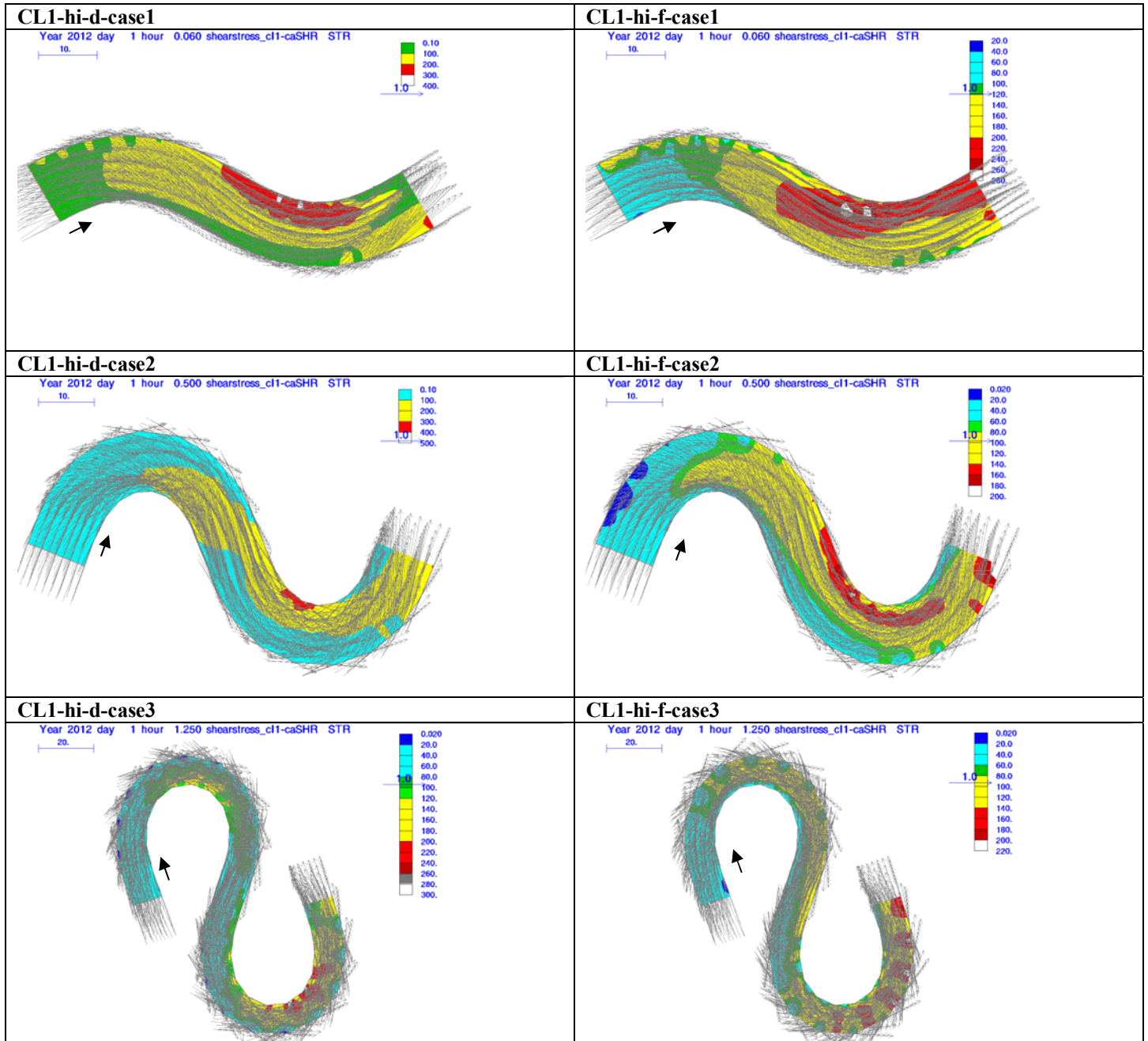


**Fig. 3** Flow structures.

Table 2. Bed shear stress



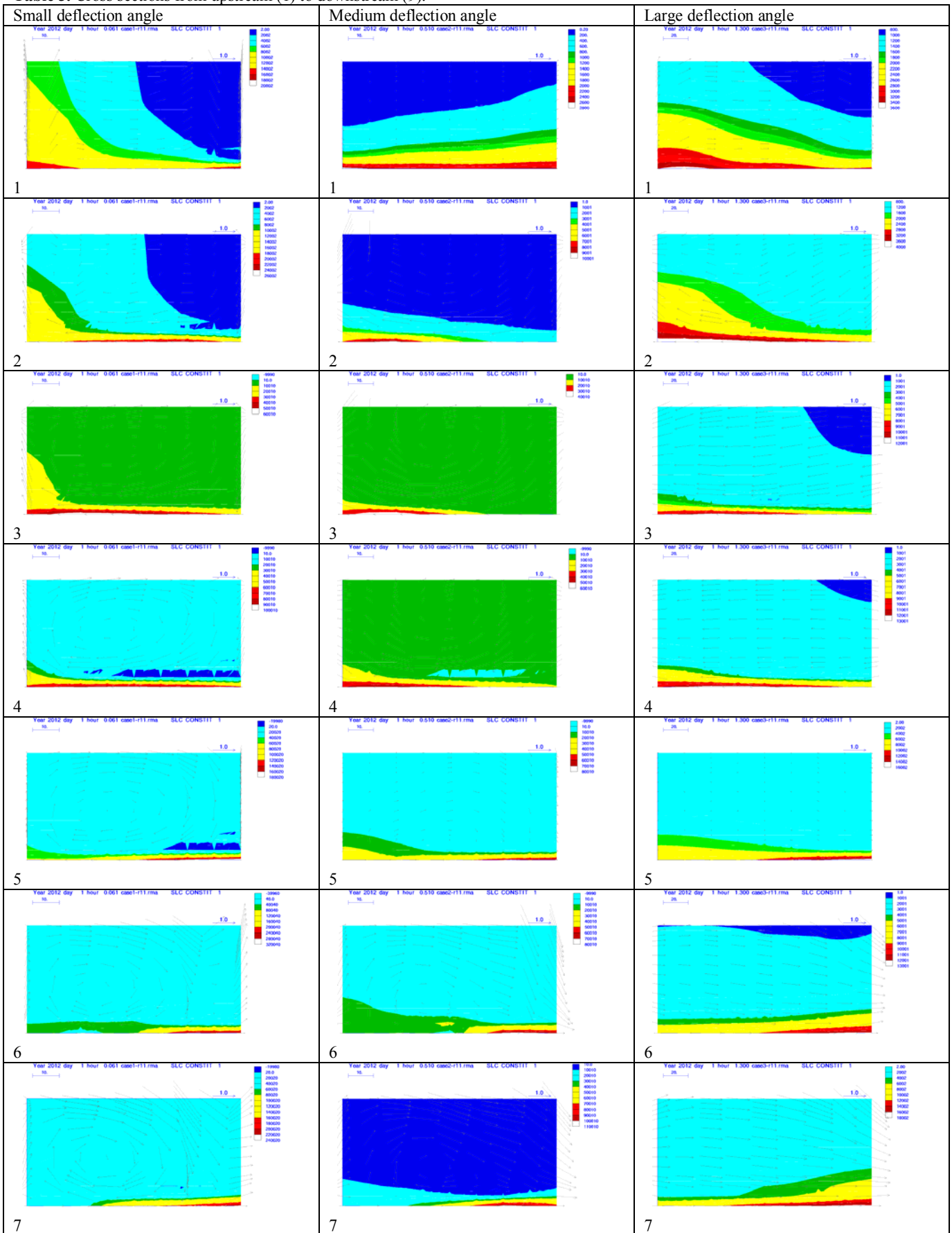
development is not as strong as for others, from cross-section 1 to 4, it spins clockwise direction but in cross-section 5 it is disappeared and then developed in counter-clockwise direction from cross-section 6 to 9.

The bed deformation affects the intensity of helical flow where the more inclined bed makes the helical flow stronger as shown in Fig. 4. According to de Vriend (1977), Julien (2003), and da Silva & el Tahawy (2008), the intensity of the flow is influenced by bed shear stress. For each of deflection angle geometry, bed is inclined maximum at  $\tan^{-1}\left(\frac{3}{11}\right) = 15.25^\circ$  where channel width is 11 m and bed height difference is 3 m. In Table 2, bed shear stress for bed deformed channels are bigger than the flat ones.

Agreed with Struikma *et al.*, (1985), Julien (2003) and Wu (2008), that the bed deformation gives significant effect in the development of helical flow since it governs the interaction between the turbulent flow motion and the suspended sediment constituting the river bed.

For depth profiles at the outer bank, bed is deepened downward displacement where erosion zones coincide with acceleration zones. At the inner bank, bed is thickened upward displacement where deposition zone correspond to deceleration zones. These are along with da Silva (2006) experiments, in Fig. 4, the erosion is happened at the high accelerated zone where the bed is deepened, and the deposition is located at the low decelerated zone where the bed is thickened.

**Table 3.** Cross sections from upstream (1) to downstream (9).



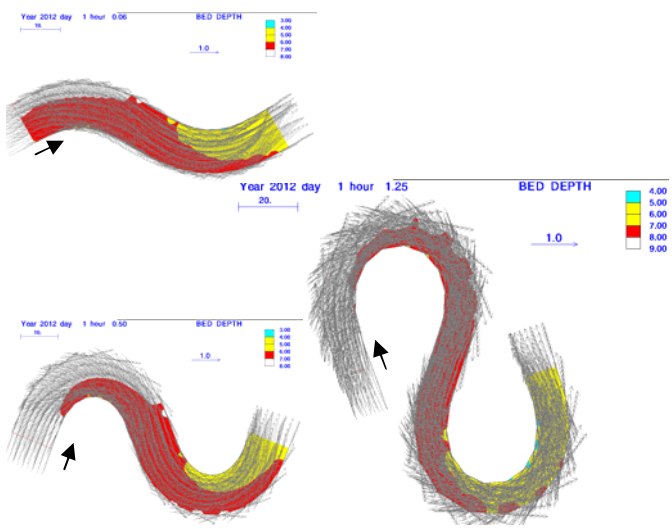
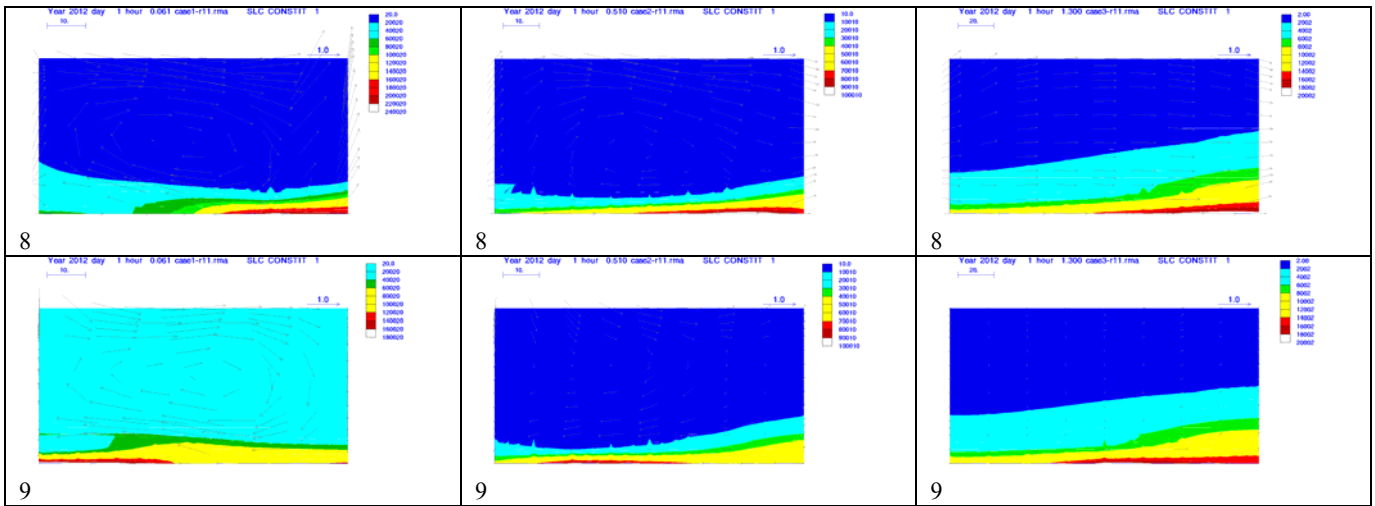


Fig. 4 Bed depths

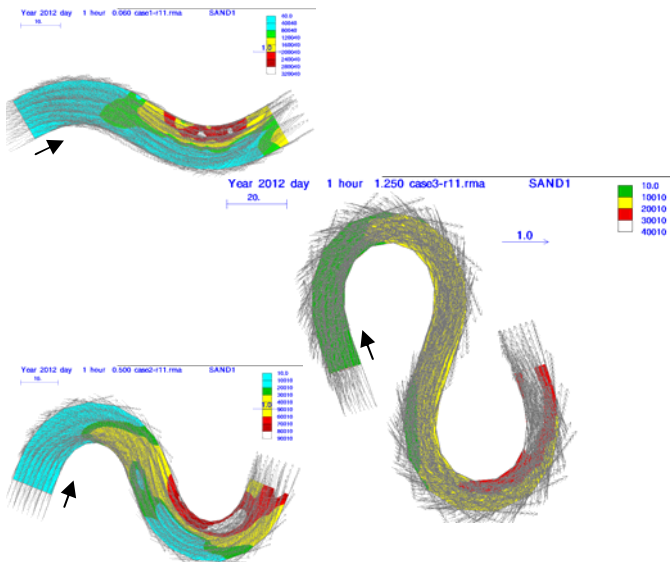


Fig. 5 Non-cohesive (Sand) sediment concentrations

Consequently, the erosion-deposition process govern the movement of meander either lateral expansion or downstream migration as referred to da Silva (2006) and Garde (2006). The process is also to vary with deflection angles, as stated by Esfahani & Keshavarzi (2012) where migration is dominating for small

deflection angle, and expansion is dominating for large deflection angle.

For sediment distribution, the highest concentration zone is located at the outer-bank where erosion occurs. The lowest concentration zone is place at the inner-bank where deposition happens, as in Fig. 5.

With the Froude number is more than thus the flow is supercritical, since at higher flow there are stronger secondary flows with maximum scour potential near the outer bank (Julien, 2003), as seen in Figs 3, 4 and 5.

About the bed erosion, it is related to the 4th and 5th point of approaches on the paper, which are (4) simulating sediment transport process due to coherent structures and burst in meandering river, and (5) modeling eroding process as mechanical interaction fluid-soil at river bank. In this paper it is shown the distribution of sediment transport along the system for non-cohesive (sand/silt) sediment.

It took sometimes to get a better flow structures results with RMA-10. It is because a reasonable result of sediment transport depends on a reasonable result of the flow structures in the system (Bates *et al.*, 2005). Meander occurs even when there is no sediment transport; meandering is caused by the large-scale turbulence (da Silva, 2006).

RMA-11 is using advection diffusion equation and erosion-deposition method for sand source/sink terms. Erosion and/or deposition are dependent on the bed shear stress developed by flowing water and the shear strength of the surface layer on the bed. Bed erosion will occur when it is above a critical level of a shear stress, and bed deposition will occur when the shear stress on the bed is not sufficient to re-suspend particles. Bed shear stress is a function of water density times to a square of shear velocity.

Julien (2003) stated when the strength of secondary circulation increases the equilibrium in river bends prevails between outer-bank erosion and inner-bank deposition. This strength has function of deviation angle of the streamlines near the bed which is a ratio of radial shear stress to the downstream bed shear stress.

The recent researches show that due to the gravitational force the flow in an open channel with a given slope would continuously accelerate, but a steady state is achieved due to friction at the bottom and the sidewalls. In other words, the equilibrium is due to a momentum transport from the flow to the walls. The momentum transport occurs in a turbulent flow, and has consequences for the transport of sediment. In a turbulent flow the exchange of momentum between different levels in the flow is mainly achieved by so-called flow structures, since the viscous contribution is rather small (Gyr, 2011). Da Silva (2006) concluded that the zones of the downward and upward bed displacements (i.e. the erosion and deposition zones) must necessarily coincide with the zones of convective acceleration and deceleration of flow which can be explained by its flow structures. These can be seen in **Table 2**, the circulation of velocity vectors at the center of the channel is different to at the inner and outer bank.

From here, we could predict the area where will occur the soil-water mechanical interaction at the erosion and deposition zones. The above simulations may have added significantly to our understanding of the controls upon secondary circulation in the type of idealized channel geometries that have commonly been investigated in laboratory experiments.

Furthermore, we could connect this finding therefore we could quantify the erosion and deposition process by exploring RMA with finite element method (FEM). Otherwise, recent studies proposed a better results with meshless numerical method such smoothed particle hydrodynamics (SPH) (Gomez-Gesteira *et al.*, 2010) where we could compare the results from RMA.

**Acknowledgment** This work is using RMA-10 version 8.7H (November 2012), RMA-11 version 8.7H (January 2013), RMAGEN version 8.1J (December 2012), and RMAPLT version 8.4G (January 2013). These codes are supported by Dr. Ian P. King, Research Modelling Associates, Sidney, NSW, Australia.

## CONCLUSIONS

Most important characteristics of meandering phenomena are dynamics of flow and transport properties, and dynamics of morphology.

In regard to dynamics of flow properties, this study has identified that the key characteristics are helical flow and coherent structures (bursts and sweeps), and higher flow velocity at the outer banks and lower in the inner banks.

With respect to dynamics of transport properties, this study has identified that the key characteristics are sediment erosion at the outer banks and deposition in the inner banks, higher sediment concentration at the outer banks and lower in the inner banks.

This work has shown that RMA is capable to simulate meander of those two characteristics.

Concerning dynamics of morphology, this study shows large deviation angle shifts the maximum velocity zones and determines the direction of channel migration to downstream.

In detail, RMA results show that for small deflection angles (30°) location of maximum erosion-deposition zones is near the crossover of the sinuosity, for intermediate deflection angles (70°) location of maximum erosion-deposition zones is between the crossover and apex of the sinuosity, and for large deflection angles (110°) location of maximum erosion-deposition zones is near the apex of the sinuosity. These are agreed with experiments of Odgaard (1989), da Silva (2006a), da Silva *et al.* (2006b) and Esfahani & Keshavarzi (2012).

But, since RMA is based on stationer grid, it is not able to simulate the meander dynamics of morphology.

Nevertheless, any effort to overcome this lack, the model has to possess the above two capabilities.

Or in other words, these results from this study can be used as reference to develop other model.

## REFERENCES

- Bates P. D., Lane S. N., and Ferguson R. I. (editors) (2005) *Computational Fluid Dynamics: Applications in Environmental Hydraulics*, John Wiley and Sons, Ltd.
- Brunner G. W. (2010) *HEC-RAS River Analysis System Hydraulic Reference Manual*, US Army Corps of Engineers, Hydrologic Engineering Center.
- Blanckaert, K., and de Vriend, H. J. (2010) Meander dynamics: A nonlinear model without curvature restrictions for flow in open-channel bends, *J. Geophys. Res.*, 115, F04011, doi:10.1029/2009JF001301.
- Camporeal, C., Perona, P. Porporato, A., and Ridolfi, L. (2007) Hierarchy of Models for Meandering Rivers and Related Morphodynamic Processes, *Rev. Geophys.*, 45, RG1001, doi:10.1029/2005RG000185.
- Corney R. K. T., Peakall J., Parsons D. R., Elliott L., Amos K. J., Best J. L., Keevil G. M., and Ingham D. B. (2006) The orientation of helical flow in curved channels, *Sedimentology* 53, 249.
- Chanson H. (2004) *Environmental Hydraulics of Open Channel Flows*, Elsevier Butterworth-Heinemann.
- da Silva A. M. F. (2006) On why and how do rivers meander, *J. Hydraul. Res.*, 44:5, 579–590.
- da Silva A. M. F., El-Tahawy, T. and Tape, W. D. (2006) Variation of Flow Pattern with Sinuosity in Sine-Generated Meandering Streams, *J. Hydraul. Eng.*, 2006. 132:1003-1014, doi: 10.1061/(ASCE)0733-9429(2006)132:10(1003).
- da Silva, A.M. F., and El-Tahawy, T. (2008) On the location in flow plan of erosion–deposition zones in sine-generated meandering streams, *J. Hydraul. Res.*, 46:S1, 49–60-49–60.
- da Silva, A. M. F. and Ahmari, H. (2009) Size and effect on the mean flow of large-scale horizontal coherent structures in open-channel flows: an experimental study, NRC Research Press, *Can. J. Civ. Eng.* 36:9, 1643-1655, doi:10.1139/L09-093.
- de Vriend, H. J. (1977): A Mathematical Model Of Steady Flow In Curved Shallow Channels, *J. Hydraul. Res.*, 15:1, 37–54, dx.doi.org/10.1080/00221687709499748.

- Duan, Jennifer G. and Julien, Pierre Y. (2010) Numerical simulation of meandering evolution, *J. Hydrology*, 391: 34–46, doi: 10.1016/j.jhydrol.2010.07.005.
- Einstein A. (1926) The Cause of the Formation of Meanders in the Courses of Rivers and of the So-Called Baer's Law, *Die Naturwissenschaften*, vol. 14.
- Esfahani, F. S. and Keshavarzi, A. (2012) Dynamic mechanism of turbulent flow in meandering channels: considerations for deflection angle, *Stoch Environ Res Risk Assess*, Springer-Verlag Berlin Heidelberg. doi: 10.1007/s00477-012-0647-0.
- Garde, R. J. (2006) *River Morphology*, New Age International (P) Ltd, Publishers.
- Gomez-Gesteira, M., Rogers, B. D., Dalrymple, R. A., Crespo, A. J. C. (2010) State-of-the-art of classical SPH for free-surface flows, *J. Hydraul. Res.*, 48, Extra Issue, 6–27.
- Güneralp, İ., Abad, J. D., Zolezzi, G., and Hooke, J. (2012) Advances and challenges in meandering channels research, *Geomorphology*, 163–164, 1–9. doi: 10.1016/j.geomorph.2012.04.011.
- Gyr, A. (2011) Old and new concepts based on coherent structures for understanding sediment transport, *Int. J. Sediment Res.*, 26:3, 378–386.
- Hussain, A.K.M.F. (1983) Coherent Structures—Reality and Myth, *Phys. Fluids*, vol. 26, Oct.
- Ji Zhen-Gang (2008) *Hydrodynamics and Water Quality: Modeling Rivers, Lakes and Estuaries*, Wiley Interscience.
- Julien, Pierre Y. (2002) *River mechanics*, Cambridge University Press.
- Keshavarzi, A. and Esfahani, F. S. (2011) Effect of different meander curvatures on spatial variation of coherent turbulent flow structure inside ingoing multi-bend river meanders, *Stoch Environ Res Risk Assess* (2011) 25:913–928, Springer-Verlag, doi: 10.1007/s00477-011-0506-4.
- King. I. P. (1993) RMA-10 A Finite Element Model for Three-Dimensional Density Stratified Flow, Department of Civil and Environmental Engineering, University of California Davis.
- King. I. P. (2012) A Finite Element Model for Stratified Flow RMA-10 Users Guide Version 8.7e, Resource Modelling Associates, Sydney, NSW, Australia.
- King. I. P. (2013) RMA-11: A Three Dimensional Finite Element Model for Water Quality in Estuaries and Streams Documentation Version 8.7H, Resource Modelling Associates, Sydney, Australia.
- Langbein, W.B. and Leopold, L.B. (1966) *River Meanders—Theory of Minimum Variance*, U.S. Geol. Survey Prof. Paper 422-H, 1–15.
- Leopold, L. B. and Wolman, M. G. (1957) *River Channel Patterns, Braided, Meandering and Straight*, Geological Survey Professional Paper 282 B, US Government Printing Office, Washington.
- Mao, Y. (2003) The Effects of Turbulent Bursting on The Sediment Movement in Suspension, *Int. J. Sediment Res.*, 18:2, 148–157.
- Odgaard, A. Jacob (1989) River-Meander Model. I: Development, *J. Hydraul. Engng*, 115, 1433–1450.
- Papanicolaou A. N. T., Elhakeem M., Krallis G., Prakash S., Edinger J. (2008) Sediment Transport Modeling Review—Current and Future Developments, Forum, *J. Hydraul. Engng ASCE*.
- Prince George's County (1999) *Low-Impact Development Design Strategies: An Integrated Design Approach*, Department of Environmental Resource, Programs and Planning Division, Maryland.
- Raudkivi, A. J. (1998) *Loose Boundary Hydraulics*, A. A. Balkema.
- Riley, James D. and Rhoads, Bruce L. (2012) Flow structure and channel morphology at a natural confluent meander bend, *Geomorphology*, 163–164: 84–98, doi: 10.1016/j.geomorph.2011.06.011.
- Sanjou M., Nezu I. (2009) Turbulence structure and coherent motion in meandering compound open-channel flows, *J. Hydraul. Res.*, 47:5, 598–610.
- Shao, S. and Gotoh, H. (2005) Turbulence particle models for tracking free surfaces, *J. Hydraul. Res.*, 43:3, 276–289.
- Struiksma N., Olesen K. W., Flokstra C. & De Vriend H. J. Dr. (1985) Bed deformation in curved alluvial channels, *J. Hydraul. Res.*, 23:1, 57–79.
- Termini, D. and Piraino, M. (2011) Experimental analysis of cross-sectional flow motion in a large amplitude meandering bend, *Earth Surf. Process. Landforms*, 36:244–256, doi: 10.1002/esp.2095.
- Tilston, M., Rennie, C., Arnott, R. W. C. and Post, G. (2009) On the Nature of Coherent Turbulent Structures in Channel Bends: Burst-Sweep Orientations in Three-Dimensional Flow Fields, 33rd IAHR Congress: Water Engineering for a Sustainable Environment, ISBN: 978-94-90365-01-1.
- van Balen, W., Uijtewaal, W. S. J., and Blanckaert, K. (2010) Large-eddy simulation of a curved open-channel flow over topography, *Physics of Fluids* 22, 075108.
- Vickers, D., Mahrt, L. and Belušić, D. (2008) Particle simulations of dispersion using observed meandering and turbulence, *Acta Geophysica*, 56(1), 234–256, doi: 10.2478/s11600-007-0041-3.
- Wendt, John F. (ed.) (2009) *Computational Fluid Dynamics: An Introduction*, 3rd Edition, A von Karman Institute Book, Springer-Verlag Berlin Heidelberg.
- Woo Hyoseop (2010) Trends in ecological engineering in Korea, *J. Hydro-environ. Res.*, 4, 269–278.
- Wormleaton, Peter R. & Ewunetu, Manaye (2006) Three-dimensional  $k-\epsilon$  numerical modelling of overbank flow in a mobile bed meandering channel with floodplains of different depth, roughness and planform, *J. Hydraul. Res.*, 44:1, 18–32.
- Wu W. (2008) *Computational River Dynamics*, Taylor and Francis Group, London, UK.